CHEMISTRY
A EUROPEAN JOURNAL

DOI: 10.1002/chem.200701316

Delicate Crystal Structure Changes Govern the Magnetic Properties of 1D Coordination Polymers Based on 3d Metal Carboxylates

Konstantin S. Gavrilenko,[a, b] Olivier Cador,[a] Kevin Bernot,[c, d] Patrick Rosa,[e] Roberta Sessoli,[c] Stéphane Golhen,[a] Vitaly V. Pavlishchuk,[b] and Lahcène Ouahab*[a]

Abstract: Homo- and heterometallic 1D coordination polymers of transition metals (Co^{II}, Mn^{II}, Zn^{II}) have been synthesized by an in-situ ligand generation route. Carboxylato-based complexes $[Co(PhCOO)_2]_n$ (**1a**, **1b**), $[Co(p\text{-MePhCOO})_2]_n$ (**2**), $[ZnMn(PhCOO)_4]_n$ (**3**), and $[CoZn(PhCOO)_4]_n$ (**4**) (PhCOOH = benzoic acid, *p*-MePhCOOH = *p*-methylbenzoic acid) have been characterized by chemical analysis, single-crystal X-ray diffraction, and magnetization measurements. The new complexes **2** and **3** crystallize in orthorhombic space groups *Pnab* and *Pcab* respectively. Their crystal structures consist of zigzag chains, with alternating M^{II} centers in octahedral and tetrahedral positions, which are similar to those of **1a** and **1b**. Compound **4** crystallizes in monoclinic space group $P2_1/c$ and comprises zigzag chains of M^{II} ions in a tetrahedral coordination environment. Magnetic investigations reveal the existence of antiferromagnetic interactions between magnetic centers in the heterometallic complexes **3** and **4**, while ferromagnetic interactions operate in homometallic compounds (**1a**, **1b**, and **2**). Compound **1b** orders ferromagnetically at $T_C = 3.7$ K whereas **1a** does not show any magnetic ordering down to 330 mK and displays typical single-chain magnet (SCM) behavior with slowing down of magnetization relaxation below 0.6 K. Single-crystal measurements reveal that the system is easily magnetized in the chain direction for **1a** whereas the chain direction coincides with the hard magnetic axis in **1b**. Despite important similarities, small differences in the molecular and crystal structures of these two compounds lead to this dramatic change in properties.

Keywords: carboxylato ligands · coordination polymers · magnetic properties · single-chain magnets

Introduction

Recently, the chemistry of coordination polymeric complexes has made rapid progress.[1] In particular, 1D ordered coordination polymers with paramagnetic metal centers have attracted growing attention on account of their remarkable combination of physical properties (for example, photoluminescence[2] and adsorption[3]).[1a] They can be employed in molecular-based electronic devices, adsorbents, and chemical sensors.[4] One-dimensional (1D) coordination

[a] Dr. K. S. Gavrilenko, Dr. O. Cador, Dr. S. Golhen, Prof. L. Ouahab
Organometallic and Molecular Materials
UMR 6226 CNRS-UR1 Sciences Chimiques de Rennes
Université de Rennes 1
263 Avenue du Général Leclerc, 35042 Rennes Cedex (France)
Fax: (+33) 2-23-23-68-40
E-mail: lahcene.ouahab@univ-rennes1.fr

[b] Dr. K. S. Gavrilenko, Prof. V. V. Pavlishchuk
L. V. Pisarzhevskii Institute of Physical Chemistry of the National Academy of Sciences of the Ukraine
Prospekt Nauki 31, 03039 Kiev (Ukraine)

[c] K. Bernot, Prof. R. Sessoli
Laboratorio di Magnetismo Molecolare & INSTM
Dipartimento di Chimica
Università degli Studi di Firenze, Polo Scientifico Universitario
Via Lastruccia n. 3, 50019 Sesto Fiorentino (Italy)

[d] K. Bernot
UMR 6226 CNRS-INSA Sciences Chimiques de Rennes
Equipe "Matériaux Inorganiques: Chimie Douce et Réactivité"
INSA-Rennes, 20 Avenue des buttes de Coësmes, CS 14315
35043 Rennes Cedex (France)

[e] Dr. P. Rosa
Groupe des Sciences Moléculaires
Institut de Chimie de la Matière Condensée de Bordeaux
UPR CNRS no. 9048, Université Bordeaux I
87 Av. Doc. A. Schweitzer, 33608 Pessac (France)

Supporting information for this article is available on the WWW under http://www.chemistry.org or from the author.

polymers may present peculiar magnetic properties, such as the opening of magnetic hysteresis loops at low temperature due to the slowing of magnetization relaxation, and behavior as so-called single-chain magnets (SCMs).[5]

Carboxylato ligands are widely exploited for construction of coordination polymers. Use of polycarboxylic acids leads to the formation of two- (2D) and three-dimensional (3D) coordination networks.[1f,6] In most cases, use of monocarboxylic acids results in creation of discrete mono- or polynuclear complexes (0D). One-dimensional complexes of first-row transition metals with solely monocarboxylic acids acting as both linkers and ligands are rare,[7] and therefore it would be interesting to develop new methods for the synthesis of such complexes and to study their properties.

In most cases, carboxylate-based coordination polymers are synthesized by solvothermal procedures.[1c,f,6] Recently we proposed[8] a convenient route for the synthesis of various homo- and heterometallic polynuclear carboxylato complexes, based on in-situ redox carboxylato ligand generation. Homometallic $[Co(PhCOO)_2]_n$ and heterometallic $[CoMn(PhCOO)_4]_n$ 1D coordination polymers of transition metals could also be synthesized easily by this route.[8a] We extended our investigations and prepared new polymeric coordination compounds. We report below the synthesis, crystal structures, and magnetic properties of several new carboxylato-bridged 1D coordination polymeric complexes, namely homo- and heterometallic $[Co(PhCOO)_2]_n$ (**1a**, **1b**), $[Co(p\text{-}MePhCOO)_2]_n$ (**2**), $[MM'(PhCOO)_4]_n$ (MM′ = ZnMn (**3b**), and CoZn (**4**). In particular, **1a** behaves as an SCM at very low temperatures.

Results and Discussion

Synthesis: The in-situ carboxylate redox generation approach has been used for the synthesis of 1D coordination polymeric complexes.[8] It has been shown that the reaction between cobalt nitrate and benzaldehyde leads to the formation of a blue solution containing "cobalt(II) benzoate".[8a] Two different $[Co(PhCOO)_2]_n$ crystal phases, monoclinic **1a** and orthorhombic **1b**, were isolated from this cobalt(II) benzoate solution, depending on crystallization conditions.[8a] We improved the method described to obtain the pure form of **1b** without accidental contamination of **1a** due to cocrystallization of the two phases. The addition of nucleator (several crystals of **1b**) in the hot cobalt(II) benzoate solution leads to crystallization of the orthorhombic form of $[Co(PhCOO)_2]_n$ alone without admixture of the monoclinic form. Both forms of cobalt benzoate decompose slowly in the moisture of the air.

Manganese and nickel coordination polymers of this type could not be prepared by the proposed method. This may be caused by a less pronounced ability of these ions, compared with cobalt, to form tetrahedral coordination centers, which is essential for formation of this type of coordination polymer (vide infra).

The chemical compositions of all the complexes were confirmed by elemental analysis. The ratio M/M′ is 1:1 in all the heterometallic complexes and is constant for different crystals of the same batch, confirming that the heterometallic 1D coordination polymers are not a mixture of homometallic complexes.

Crystal structures of the two modifications of $[Co(PhCOO)_2]_n$ (1a, 1b): The structures of the monoclinic[7a] *C*2/*c* (**1a**) and orthorhombic[8a] *Pcab* (**1b**) forms of $[Co(PhCOO)_2]_n$ have already been described briefly. These two modifications have very different magnetic behaviors. To explain these differences, we compare their crystal structures in detail here. The structures of both **1a** and **1b** are built up from neutral $[Co(PhCOO)_2]_n$ zigzag chains consisting of cobalt ions in alternating tetrahedral (Co_{tetr}) and octahedral (Co_{oct}) polyhedra (Figure 1). The chains lie along the *c* and

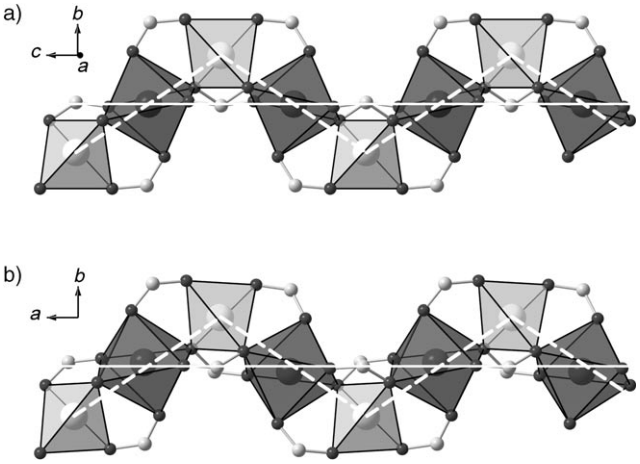

Figure 1. The chain structures in **1a** (a) and **1b** (b) with cobalt coordination polyhedra.

a crystallographic directions for **1a** and **1b**, respectively.[7a,8a] In **1a** both Co_{oct} and Co_{tetr} occupy special positions giving rise to a unique $Co_{oct}\cdots Co_{tetr}$ distance (3.151(1) Å), whereas in **1b** the metal ions are in general positions and yield two different $Co_{oct}\cdots Co_{tetr}$ distances (3.166(1) and 3.196(1) Å). Thus, the chain structure of **1a** is built of a regular zigzag motif, whereas in **1b** the chain consists of a regular double zigzag motif (Figure 1). In the crystal lattice of **1a** the chains are well isolated from each other (see Figure 2a) with neither π–π interactions nor short interchain contacts in the order of magnitude of the sum of the van der Waals radii. Short intrachain contacts between carbon atoms of aromatic rings of $\mu_2(\eta_1,\eta_1)$-benzoates exist in complex **1a**, **1b**, and also **2**. This type of contact certainly contributes to the chain stability. Also, the neighboring chains in the lattice of **1b** are not related by simple lattice translation but they are related by glide planes and therefore they have different relative orientations (see Figure 2b). As a result, short interchain contacts (3.297 Å) exist between carbon atoms C24; the

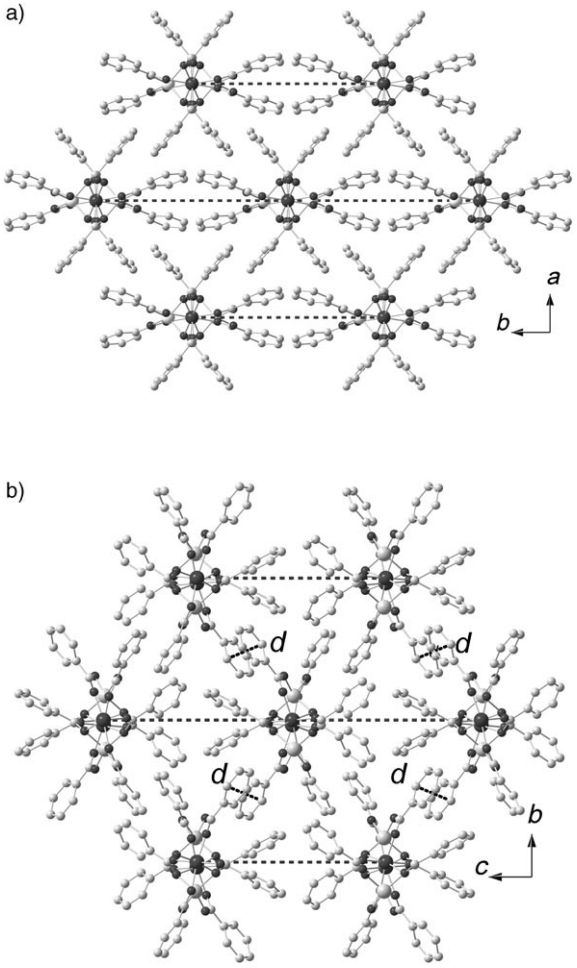

Figure 2. Crystal packing in the plane perpendicular to the chain axis in a) **1a**; b) **1b**. The interchain distances between metal sites along the *b* and *c* directions, represented by dotted lines, are 14.161(1) Å in **1a** and 12.672(1) Å in **1b**. Label *d* represents close contacts (C24···C24) between chains in **1b**.

chains are closer in **1b** than in **1a**. Indeed, the packing of the chains is more compact in **1b** than in **1a** in the *b* and *c* directions, respectively (see Figure 2). The shortest interchain $Co_{tetr}\cdots Co_{tetr}$ distance in **1a** is 10.303(9) Å, which is accidentally equal to the shortest interchain $Co_{tetr}\cdots Co_{oct}$, whereas in **1b** it is 9.067(1) Å. Finally, the crystal packing of complex **1b** is more compact ($\rho_{calcd} = 1.605\ g\,cm^{-3}$) than that of **1a** ($\rho_{calcd} = 1.557\ g\,cm^{-3}$).

Molecular and crystal structures of 1D coordination polymers 2, 3, and 4: Selected labeled drawings of compounds **2**, **3**, and **4** are shown in Figures 3, 4, and 5, respectively. Selected bond lengths and angles are given in Table 1.

The complex $[Co(p\text{-}MePhCOO)_2]_n$ (**2**) crystallizes in the orthorhombic space group *Pnab* (Table 2). As in **1a**, its structure consists of similar zigzag chains which run along the *a* direction. Surprisingly, the detailed chain structure of **2** is more similar to the monoclinic form **1a** than to the orthorhombic **1b**. The two metal sites are indeed located in special positions. The Co1 and Co2 atoms of the asymmetric unit are connected by three bridging *p*-methylbenzoato anions (Figure 3a). One carboxylato possesses the $\mu(\eta_1\text{-}O3,\eta_1\text{-}O4)$ coordination mode and is very close to the plane (*ab*) containing the zigzag chains. Two other bridges between Co1 and Co2 are formed by $\mu_3(\eta_1\text{-}O1,\eta_2\text{-}O2)$-*p*-methylbenzoato ligands, which are connected to a third metal ion ($Co1^{i}$) in the chain. They are very close to the plane (*ac*) perpendicular to the zigzag chains. The cobalt ions are located alternately in distorted tetrahedral ($Co1O_4$) and octahedral ($Co2O_6$) coordination polyhedra, which are formed by oxygen atoms of *p*-methylbenzoato bridges. Two different Co1–O bond lengths are found in the $Co1O_4$ tetrahedron (Co1–O4 is 1.938(2) and Co1–O2 is 2.036(1) Å). The angles O-Co1-O range from 94.41(10)° to 120.13(7)° (see Table 1). Three Co2–O bond lengths are observed in the octahedron $Co2O_6$ (Co2–O3 is 2.016(2), Co2–O1 is 2.115(2), and Co2–O2 is 2.219(1) Å) and the corresponding angles range from 84.50(6)° to 95.50(6)°. The observed values are closer to the corresponding distances in **1a** than to those in **1b**. $Co2_{oct}$ is located in a special position leading to a unique $Co2_{oct}\cdots Co1_{tetr}$ intrachain distance of 3.157(1) Å. Additionally, the chains in **2** are more elongated (chain period 10.532(3) Å) than in complexes **1a** and **1b** (10.48(1) and 10.503(3) Å, respectively). Moreover, cobalt ions in the octahedral positions are not displaced in this structure and form a straight line along the *a* axis (see Figure 3b). The shortest interchain Co···Co distance in complex **2** is more than 11 Å and longer than those observed in both **1a** and **1b**. This is possibly due to the presence of the CH_3 substituent on the aromatic ring of the *p*-methylbenzoato bridges in **2**. As a result, the crystal packing of complex **2** is less compact ($\rho_{calcd} = 1.450\ g\,cm^{-3}$) than in **1a** and **1b.**

The heterometallic complex $[ZnMn(PhCOO)_4]_n$ (**3**) crystallizes in the orthorhombic space group *Pcab* (Table 2). This compound is isostructural with $[CoMn(PhCOO)_4]_n$,[8a] with diamagnetic Zn^{II} instead of paramagnetic Co^{II} in the tetrahedral position. These 1D chains run along the *a* direction. There are four independent benzoato bridges in this compound (see Figure 4). The Mn1 and Zn1 ions are connected by three different bridges: the first is formed by the $\mu(\eta_1\text{-}O3,\eta_1\text{-}O4)$-benzoato ligand, and the second and the third are formed by the $\mu_3(\eta_1\text{-}O5,\eta_2\text{-}O6)$-benzoato and the η_2-O1 oxygen atom of the $\mu_3(\eta_1\text{-}O2,\eta_2\text{-}O1)$ ligand. The fourth $\mu(\eta_1\text{-}O7,\eta_1\text{-}O8)$ ligand connects Zn1 to the symmetry-related Mn atom. Four oxygen atoms of bridging benzoato ligands form a distorted tetrahedral ZnO_4 coordination polyhedron. All the Zn1–O bond lengths are different (ranging from 1.930(3) to 2.060(3) Å) and are in agreement with those found in the homometallic 1D coordination polymer $[Zn(PhCOO)_2]_n$,[7b] where zinc ions have a similar tetrahedral coordination environment. The O-Zn1-O angles vary from 101.87(13)° to 115.67(12)°. Mn^{II} atoms are located in a highly distorted $Mn1O_6$ octahedral coordination environment with three pairs of significantly different Mn1–O distances: 2.095(3) and 2.109(3), 2.201(3) and 2.211(3), 2.270(2) and 2.320(3) Å (see Table 1). Values for the two shorter pairs are in the range of those observed in other coordina-

Table 1. Selected distances [Å] and angles [°] for complexes **2**, **3** and **4**.

		2[a]			
Co1–O4	1.938(2)	O4-Co1-O4^{ii}	94.41(10)	O2-Co2-O3^{i}	86.82(6)
Co1–O2	2.036(1)	O4-Co1-O2	106.01(7)	O1-Co2-O3^{i}	88.95(6)
Co2–O3	2.016(2)	O2-Co1-O2^{ii}	110.15(9)	O3-Co2-O1	91.05(6)
Co2–O1	2.115(2)	O4-Co1-O2^{ii}	120.13(7)	O3-Co2-O2	93.18(6)
Co2–O2	2.219(1)	O1-Co2-O2	84.50(6)	O1-Co2-O2^{i}	95.50(6)
		3[b]			
Zn1–O4	1.930(3)	O4-Zn1-O7	101.87(13)	O5-Mn1-O2^{i}	178.52(10)
Zn1–O7	1.961(3)	O4-Zn1-O1	106.37(12)	O3-Mn1-O6^{i}	90.06(11)
Zn1–O1	2.013(3)	O7-Zn1-O1	114.75(12)	O8^{i}-Mn1-O6^{i}	87.48(10)
Zn1–O6	2.060(3)	O4-Zn1-O6	115.67(12)	O5-Mn1-O6^{i}	94.92(10)
Mn1–O3	2.095(3)	O7-Zn1-O6	114.54(11)	O2^{i}-Mn1-O6^{i}	83.67(10)
Mn1–O8^{i}	2.109(3)	O1-Zn1-O6	103.77(11)	O3-Mn1-O1	96.91(11)
Mn1–O5	2.201(3)	O3-Mn1-O8^{i}	170.45(12)	O8^{i}-Mn1-O1	85.57(10)
Mn1–O2^{i}	2.211(3)	O3-Mn1-O5	87.34(11)	O5-Mn1-O1	85.00(10)
Mn1–O6^{i}	2.270(2)	O8^{i}-Mn1-O5	83.68(12)	O2^{i}-Mn1-O1	96.45(10)
Mn1–O1	2.320(3)	O3-Mn1-O2^{i}	92.20(12)	O6^{i}-Mn1-O1	173.01(9)
		O8^{i}-Mn1-O2^{i}	96.69(12)		
		4			
M2–O2	1.930(3)	O7 M1-O6	99.22(9)	O2 M2-O5	109.56(10)
M2–O5	1.931(2)	O7 M1-O3	114.91(11)	O2 M2-O4	112.55(12)
M2–O4	1.936(3)	O6 M1-O3	105.61(11)	O5 M2-O4	112.74(11)
M2–O8	1.943(2)	O7 M1-O1	119.07(11)	O2 M2-O8	113.56(12)
M1–O7	1.929(2)	O6 M1-O1	110.97(10)	O5 M2-O8	97.10(10)
M1–O6	1.932(2)	O3 M1-O1	106.18(10)	O4 M2-O8	110.41(12)
M1–O3	1.933(3)				
M1–O1	1.942(2)				

[a] For **2**, [i]: 2–x, –y, –z; [ii]: 1.5–x, y, –z. [b] For **3**, [i]: 0.5+x, 0.5–y, z.

tion polymers such as $[MnCu(mal)_2(H_2O)_4]$[9] (mal = malonato) and linear trinuclear carboxylato complexes $[Mn_3(RCO_2)_6(L)_2]$. [10] The longest Mn1–O bonds are formed with η_2-O atoms. This significant elongation with respect to usually observed values is probably caused by the coordination of this benzoato bridge to three different metal ions (two Mn and one Zn). O-Mn1-O angles vary from 83.67(10)° to 96.91(11)° (see Table 1). The intrachain Zn1···Mn1 distances are 3.311(1) and 3.254(1) Å, and the shortest Mn1···Mn1 distance is 5.347(1) Å. Thus, there is a regular double zigzag chain structure in this compound. The chain period (10.671(1) Å) is very close to that found in the heterometallic complex $[CoMn(PhCOO)_4]_n$ (10.676(1) Å).[8a] The shortest Mn···Zn interchain distance (9.917(1) Å) and calculated density ($\rho_{calcd} = 1.575\ g\,cm^{-3}$) are also similar to those of the heterometallic CoMn compound.

Complex $[CoZn(PhCOO)_4]_n$ **4** crystallizes in the monoclinic space group $P2_1/c$ (Table 2) and is isostructural with $[Zn(PhCOO)_2]_n$.[7b] The crystal lattice comprises chains which run along the b direction and consist of $[CoZn(PhCO_2)_3]^+$ dimeric units (Figure 5). However, the Co and Zn are randomly distributed over the two metal sites M1 and M2 (see the Experimental Section for further details). Three $\mu(\eta_1$-*syn*,η_1-*syn*)-benzoato groups (O1,O2; O3,O4; and O7,O8) bridge the metal ions within a dimeric unit, while the fourth benzoato ion bonds dimer fragments in the $\mu(\eta_1$-*syn*-O5,η_1-*anti*-O6) mode. Thus, both ions are located in MO_4 tetrahedral coordination geometry. The M–O bond lengths (from 1.930(3) to 1.942(2) Å) and angles (from 97.10(10)° to 119.07(11)°) are very similar for both positions.

Magnetic properties: Magnetization of a powdered sample of **3** has been measured in the 2–300 K range. At room temperature $\chi_M T = 4.43\ cm^3\,K\,mol^{-1}$, in good agreement with the expected spin-only value ($4.375\ cm^3\,K\,mol^{-1}$) for isolated noninteracting Mn^{II} ($S_{Mn} = 5/2$) spins with $g_{Mn} = 2.0$. Upon cooling, χ_M increases and passes through a broad maximum at $T_{max} = 3.5$ K characteristic of antiferromagnetic superexchange intrachain interaction between Mn^{II} spins. The superexchange interaction between octahedral sites takes place through the two $\mu(\eta_1$-*syn*,η_2-*anti*)-benzoato bridges (see Figure 4). The experimental data can be fitted with the theoretical expression derived by Fisher[11] for an infinite chain of classical spins with the spin hamiltonian $\mathscr{H} = -J\boldsymbol{S_A}\cdot\boldsymbol{S_B}$ taking into account nearest-neighbor superexchange interactions. This expression has been modified slightly to take into account interchain interactions (zJ') through molecular-field approximation. The best agreement between experiment and theory was obtained with $J = -0.55\ cm^{-1}$, $g_{Mn} = 1.98$, and $zJ' = -0.06\ cm^{-1}$ with agreement factor $R^2 = 0.99981$ (see Supporting Information).

The magnetic behavior of **4** is more complex. Indeed, paramagnetic Co^{II} atoms are distributed randomly over the two metallic sites. Therefore, isolated tetrahedral Co^{II} (one Co^{II} bridged to two Zn^{II}) and Co^{II} chain fragments of various lengths coexist and contribute differently to the overall magnetism of the chain. The magnetic susceptibility can be fitted with the Curie–Weiss law above 100 K with $g_{Co} = 2.31$ ($S_{Co} = 3/2$) and $\theta = -25$ K, in agreement with previously reported values for tetrahedral Co^{II}.[12]

The magnetism of the homometallic 1D chain compounds $[Co(PhCOO)_2]_n$ (**1a** and **1b**) has been investigated in more detail. Above 20 K **1a** and **1b** powders revealed similar magnetic behaviors. Both compounds obey the Curie–Weiss law above 20 K with Curie constants (C) of 5.97 (6.06) $cm^3\,K\,mol^{-1}$ and Weiss temperatures (θ) of +2.87 (+7.27) K for **1a** (**1b**) with $R^2 = 0.99996$ (0.99993). Assuming a Zeeman factor for a tetrahedral Co^{II} site of $g_T = 2.31$ (as in **3**) and $S_T = 3/2$, the Zeeman factor g_O for octahedral Co^{II} was estimated to be 2.72 (2.75). The positive Weiss temperatures clearly indicate that strong ferromagnetic interac-

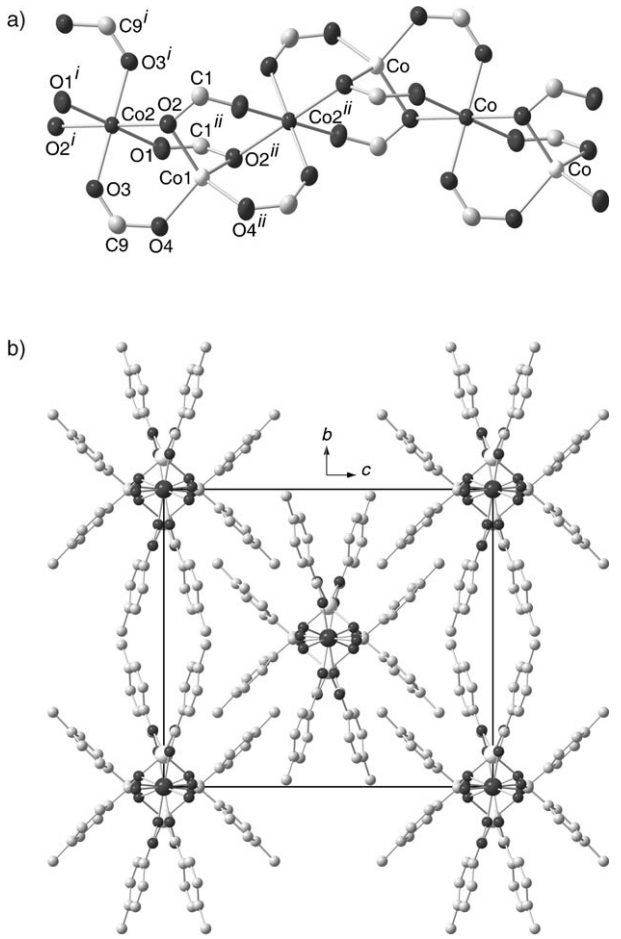

Figure 3. a) A fragment (with 50% thermal ellipsoids) of the polymer **2** showing the complete connectivity to Co1 and Co2 atoms. Phenyl rings and hydrogen atoms are omitted for clarity. b) Crystal packing in the *bc* plane (perpendicular to the chain axis).

Table 2. Crystal data and structure refinement parameters for compounds **2**, **3**, and **4**.

	2	**3**	**4**
empirical formula	$C_{16}H_{14}CoO_4$	$C_{28}H_{20}ZnMnO_8$	$C_{28}H_{20}CoZnO_8$
formula weight	329.20	604.75	608.74
T [K]	293(2)	293(2)	293(2)
crystal system	orthorhombic	orthorhombic	monoclinic
space group	*Pnab*	*Pcab*	$P2_1/c$
a [Å]	10.5320(2)	10.6710(1)	10.7236(3)
b [Å]	16.1162(3)	19.1088(3)	13.0269(3)
c [Å]	17.7628(4)	25.0140(4)	19.1120(8)
β [°]	90	90	95.579(1)
V [Å^3]	3014.98(11)	5100.6(1)	2657.2(2)
Z	8	8	4
ρ_{calcd} [g cm^{-3}]	1.450	1.575	1.522
unique reflns	5246	5858	4508
R(int)	0.0481	0.0296	0.0252
GOF on F^2	0.994	1.068	1.052
R_1[a] [$I>2\sigma(I)$]	0.0467	0.0575	0.0387
wR_2[b]	0.1115	0.1751	0.0941

[a] $R_1=\Sigma||F_o|-|F_c||/\Sigma|F_o|$. [b] $wR_2=\{\Sigma[w(F_o^2-F_c^2)^2]/\Sigma[w(F_o^2)^2]\}^{1/2}$.

tions operate between the octahedral and tetrahedral sites. Indeed, for uncoupled Co^{II} in octahedral or tetrahedral environments the magnetic susceptibility, χ_M, deviates significantly from the Curie law with negative Weiss temperatures due to local magnetic anisotropies. Therefore, to compensate for this effect, strong ferromagnetic interactions must exist between magnetic centers. The temperature dependencies of $\chi_M T$ below 50 K (Figure 6) demonstrate the ferromagnetic nature of the chains in **1a** and **1b** with the increase in $\chi_M T$ on lowering the temperature. In both **1a** and **1b**, and also in **2**, the main superexchange pathway between the octahedral and tetrahedral sites is probably through η_2-O atoms. The Co_T-η_2-O-Co_O angles range from 95.56(9)° to 97.24(7)° and are expected to produce ferromagnetic contributions.[13] Whereas $\chi_M T$ of **1a** increases monotonically on lowering the temperature to 2 K, $\chi_M T$ of **1b** increases faster and shows a cusp at 4 K which can be ascribed to the onset

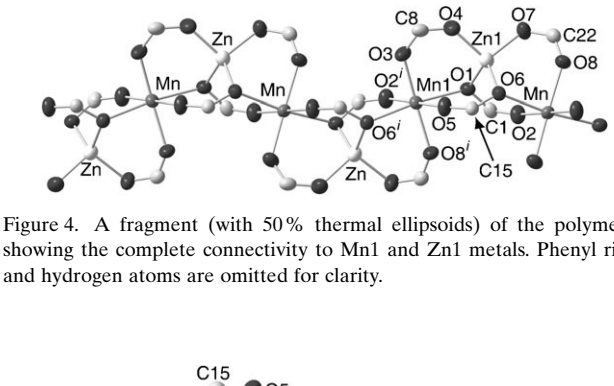

Figure 4. A fragment (with 50% thermal ellipsoids) of the polymer **3** showing the complete connectivity to Mn1 and Zn1 metals. Phenyl rings and hydrogen atoms are omitted for clarity.

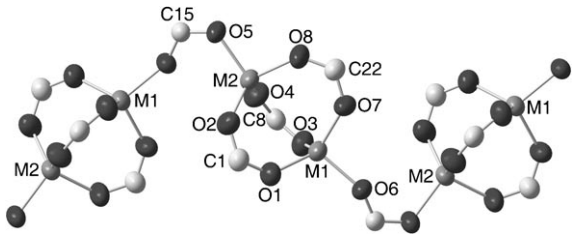

Figure 5. A fragment (with 50% thermal ellipsoids) of the polymer **4** showing the complete connectivity to M1 and M2 metals (Co and Zn are distributed randomly aver M1 and M2). Phenyl rings and hydrogen atoms are omitted for clarity.

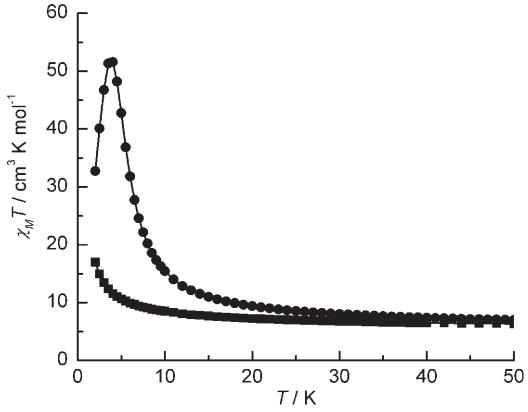

Figure 6. Thermal variation of the $\chi_M T$ product of powders of **1a** (■) and **1b** (●). Full lines are only to guide the eye.

of long-range ferromagnetic order. The existence of a ferromagnetic phase at low temperature is confirmed by the divergence between the magnetization measured in zero field cooled (ZFC) and field cooled (FC) modes (Figure 7). Also, the out-of-phase component of the AC susceptibility sud-

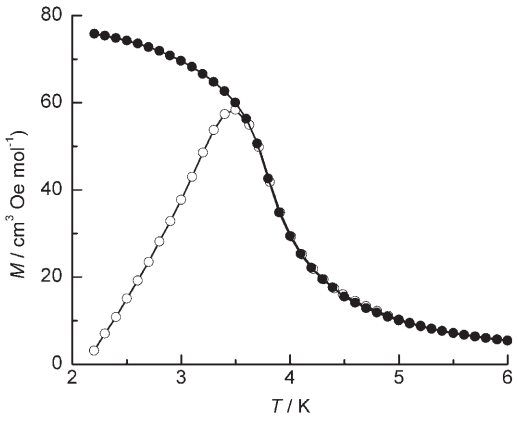

Figure 7. Temperature dependence of the magnetization of powders of **1b** measured in zero-field cooled (○) and field-cooled (●) modes with a 5 G magnetic field.

denly becomes nonzero at $T_C = 3.7$ K, which confirms 3D long-range magnetic ordering. The occurrence of long-range ordering in this 1D system is connected directly to interchain interactions. In quasi 1D systems T_C is related to intra- and interchain interactions through $k_B T_C \approx |J_{inter} \times J_{intra}|^{1/2}$, with J_{inter} and J_{intra} the intrachain and interchain interaction parameters, respectively. The orthorhombic phase (**1b**) orders ferromagnetically in the temperature range studied, whereas the monoclinic phase (**1a**) does not, either ferromagnetically or antiferromagnetically. In **1b**, the intrachain interactions are stronger than in **1a**, resulting in different Weiss temperatures. The interchain interactions are also stronger in **1b** because the interchain metal–metal separation is significantly shorter than in **1a**. For symmetry reasons, the interchain contact between aromatic rings should favor antiferromagnetic interchain interactions of superexchange origin, and not ferromagnetic ordering. Then, the magnetic ordering in **1b** is a combination of stronger intrachain interactions and stronger interchain dipolar interactions.

Complex **2** behaves like **1a** with, above 20 K, $C = 5.70\ cm^3 K mol^{-1}$ and $\theta = 1.18$ K ($R^2 = 0.99993$). It does not show magnetic ordering down to 1.8 K. As expected, the interchain interactions are smaller than in **1a** and **1b** because of longer interchain metal–metal distances (>11 Å) in this compound than in both forms of **1**; this is due to the presence of *p*-methyl substituents on the aromatic rings of the benzoates.

The strong magnetic anisotropy due to the presence of Co^{II} in both environments is confirmed by single-crystal measurements of the magnetization of **1a** and **1b**. Above 2 K, the magnetization of **1a** is much stronger when the magnetic field is applied along the *c* axis (the chain axis). In Figure 8 the temperature dependences of $\chi_M T$ are plotted versus the magnetic field, *H*, applied parallel and perpendicular to the chain axis. Whereas $\chi_M T$ decreases smoothly

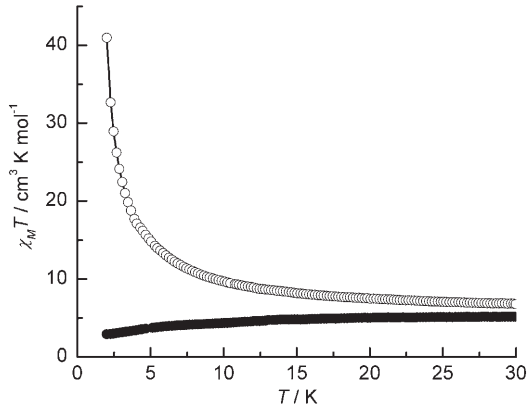

Figure 8. Temperature dependence of the $\chi_M T$ product of single crystals of **1a** with an external DC field of 100 G below 10 K and 1000 G above 10 K, applied parallel (○) and perpendicular (●) to the chain axis.

below 25 K in the perpendicular direction, it increases very rapidly in the parallel one. At 2 K, the response along the *c* axis is more than ten times greater than in the perpendicular direction. This behavior is characteristic for Ising-type ferromagnetic chains and is confirmed by low-temperature magnetization measurements. Figure 9 demonstrates clearly that

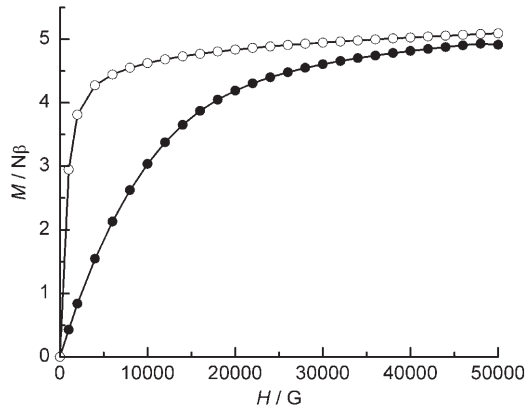

Figure 9. Field dependence of the magnetization of single crystals of **1a** at $T = 2$ K with the magnetic field parallel (○) and perpendicular (●) to the chain axis.

the magnetization saturates in a small field along the chain axis, whereas an intense field of several tesla is required to achieve saturation in a perpendicular direction. Thus the following conditions for the observation of SCM behavior are fulfilled: a) the chains are ferromagnetic with strong intrachain coupling between spin centers; b) the strong magnetic anisotropy is axial. However, no slowing of the magnetization can be detected down to 1.8 K.

To shed light on the magnetic behavior of this compound, magnetic measurements were performed at very low temperature using a ^{3}He-cooled cryostat equipped with a homemade AC probe operating in the range 20-15 000 Hz. This type of measurement combines the advantage of investigating low-temperature regions with the possibility, by looking at the out-of-phase contribution to the magnetization, of characterizing the possible slow relaxation process (that is, of establishing the presence of an SCM or a spin-glass behavior).[14] Measurements were performed in the range 330–1650 mK using 12 logarithmically spaced frequencies (from 30 to 9000 Hz). As shown in Figure 10, the lowest frequency

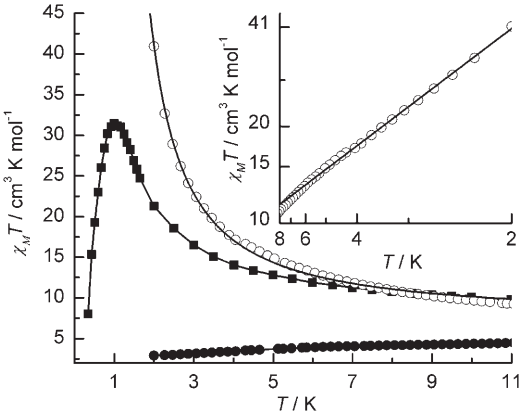

Figure 10. Temperature dependence of the $\chi_M T$ products of **1a**. Squares, extracted from SQUID measurement and from the lowest frequency of the ^{3}He AC measurement (powders). Circles represent the susceptibility along and perpendicular to the chain, as explained in Figure 8. Inset: scaling of the data using an Ising temperature dependence of the susceptibility (see text) and plotting $\ln(\chi_M T)$ versus T^{-1}. Squares and circles are data recorded on powder and on a single crystal respectively, with the magnetic field applied along the chain axis. The solid lines represent the best linear fits.

used in the ^{3}He measurements rescales well on the SQUID data, showing a $\chi_M T$ value at 1.65 K of about 24.7 cm^3 K mol^{-1}. When the temperature is lowered $\chi_M T$ continues to increase to a maximum of 31.5 cm^3 K mol^{-1} at 1 K. Such a low-temperature increase of $\chi_M T$ suggests the presence of ferromagnetic short-range order in the material. A simple way to model this behavior is to characterize the exponential divergence of the correlation length. In a ferromagnetic Ising chain, the $\chi_M T$ product should show an exponential divergence at low temperature, such as $\chi_M T \propto \exp(2JS^2/k_B T)$ where J is the exchange coupling constant between nearest neighbors.[15,5e] Then plotting $\ln(\chi_M T)$ versus 1/T should afford a straight line with the slope providing two times the exchange energy. A fit to the curve recorded for powder samples gives a JS^2 value of about 0.77 K, while along the easy axis $JS^2 = 1.66$ K (Figure 10, inset). This is a rough estimate of the exchange interaction, however. To characterize the system better, we have employed a model which assumes a genuine spin $S = 3/2$ for tetrahedral Co^{II}, whereas for octahedral Co^{II} a highly anisotropic effective spin $s = 1/2$ is more appropriate at low temperature due to the combined effects of spin–orbit coupling and distortions of the coordination sphere.[16] Curely et al. developed a model for chains with quantum spin $s = 1/2$ alternating with classical spin S for Ising-type nearest-neighbors exchange interaction, $H = -JS_i^z \cdot s_i^z$.[17] The thermal variation of the molar magnetic susceptibility is expressed as Equation (1).

$$\chi_{M_z} = \frac{Ng_S\beta^2}{4k_B T}\left[\left(\frac{4g_S{}^2S^2 + g_s{}^2}{g_s{}^2}\right)\cosh\left(-\frac{JS}{k_B T}\right) - \frac{4g_S S}{g_s}\sinh\left(-\frac{JS}{k_B T}\right)\right] \quad (1)$$

With g_s and g_S the Zeeman factors of the quantum and classical spins respectively, the constants have their usual meanings. The best-fit curve is obtained with $g_s = 5.34(5)$ and $J = 2.33(3)$ K (see Figure 10). To converge properly, g_S has been fixed at 2.31. This provides an exchange energy of 1.75 K, not very far from the value deduced from the slope of the $\ln(\chi_M T)$ versus $1/T$ curve.

Below 0.6 K, a frequency-dependent signal appears (Figure 11) and the out-of-phase susceptibility χ_M'' shows a very sharp increase from almost 0 to 10 cm^3 mol^{-1} for the highest frequency. At 0.33 K, χ_M' and χ_M'' are of the same order of magnitude.

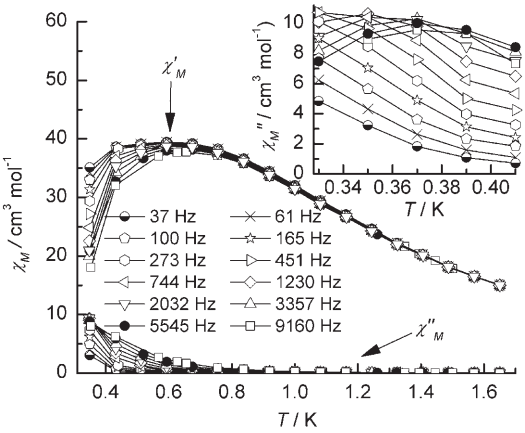

Figure 11. Temperature dependence of the imaginary χ''_M and real χ'_M components of the AC susceptibility of **1a** measured in zero applied field for 12 logarithmically spaced frequencies in the range 30–9000 Hz. Inset: temperature dependence of imaginary component χ''_M for the lowest available temperatures.

To further the analysis, the frequency dependence has been analyzed by an Arrhenius plot. The dynamic behavior of 1D systems involving Ising-type magnetic centers was explained by Glauber in the 1960s.[18] He predicted that such chains should show an exponential divergence of the relaxation time at low temperature, which can be written as $\tau = \tau_0 \exp(\Delta/k_B T)$ where Δ is proportional to the exchange energy between two adjacent spins. Values extracted from the Arrhenius plot (Figure 12) are $\Delta = 5.5 \pm 0.4$ K and $\tau_0 = (1.1 \pm 2.5) \times 10^{-11}$ s, which are in good agreement with those previously reported in the literature for similar systems.[19,5g,h]

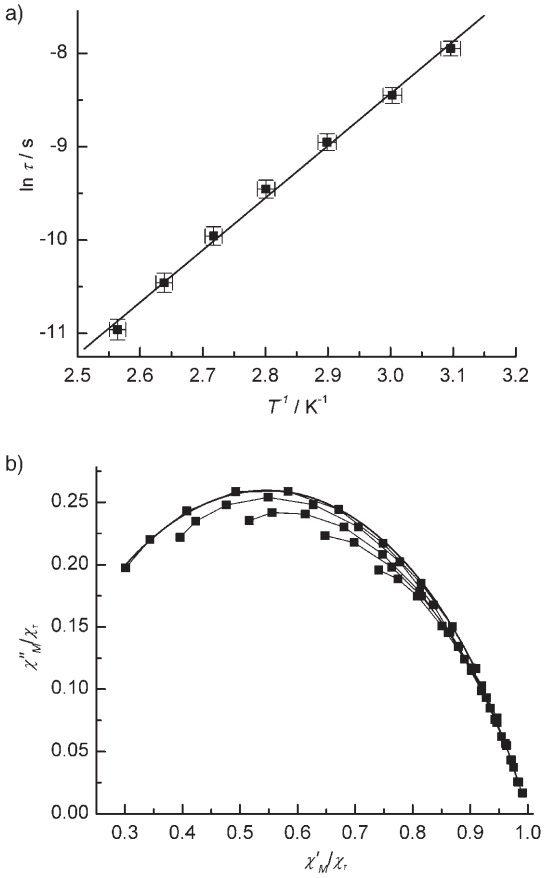

Figure 12. a) Arrhenius plot extracted for **1a**. The solid line represents linear regression. b) Argand diagram in the 30–9000 Hz frequency range. All values are normalized by the isothermal susceptibility. The solid line represents the fit at the lowest temperature (0.33 K).

Another useful tool in the analysis of the frequency dependence is the extended Debye model, which makes it possible to evaluate the assumption that the relaxation process is described by a single characteristic time. This analysis can be done by introducing a parameter α, proportional to the width of the distribution of the relaxation times, into the expression [Eq. (2)] for the complex susceptibility.

$$\chi(\omega) = \chi_S + \frac{\chi_T - \chi_S}{1 + (i\omega\tau)^{1-\alpha}} \qquad (2)$$

Here χ_T is the isothermal susceptibility, χ_S the adiabatic susceptibility, ω the frequency of the AC field and τ the relaxation time of the system at the temperature at which the fit is performed.[20] Consequently an ideal SCM or single-molecule magnet (SMM) is likely to possess a single relaxation time ($\alpha = 0$) whereas a spin glass[21] would show a wide range of relaxation process ($\alpha \rightarrow 1$). The experimentally determined Argand plot (Figure 12) is normalized by χ_T to allow easy comparison. The fitting procedure afforded $\alpha = 0.34 \pm 0.01$ at 0.33 K and similar values for the entire temperature region where frequency dependence is observed. In any case the τ_0 and α values extracted from the out-of-phase susceptibility data allow us to assess that we are not faced with a spin-glass behavior; indeed the chains are still magnetically insulated one from another at temperatures as low as 0.33 K. It is interesting to compare whether the exponential divergence of the correlation length observed in the static susceptibility compares well with the energy barrier for the reversal of magnetization. In the Glauber model the relaxation time diverges as the square of the correlation length, $\tau = \tau_0 \xi^2$. The energy barrier of the Arrhenius plot is therefore expected to correspond to twice of slope of the ln($\chi_M T$) versus $1/T$ curve. This would give an energy barrier of 6.6 K, which is not too far from the observed value of 5.5 K, considering also that the easy axes of cobalt sites along the chains are not necessarily collinear in this crystal symmetry.

The magnetic properties of single crystals of **1b** at low temperatures differ drastically from those of **1a**. Unexpectedly, the chain axis in **1b** is no longer the easy axis, but the hard axis. Upon cooling, $\chi_M T$ increases very rapidly when the applied field is perpendicular to the chain axis and decreases below T_C (Figure 13). In the ferromagnetic phase the magnetization is constant (Figure 13, inset), then the MT product (or $\chi_M T$) shows a cusp at T_C. Single-crystal measurements confirm that **1b** orders at $T_C = 3.7$ K, the magnetization standing preferentially in a plane perpendicular to the chain axis.

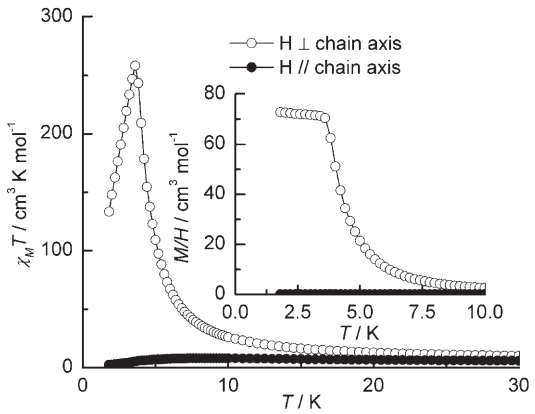

Figure 13. Temperature dependence of $\chi_M T$ of single crystals of **1b** with the magnetic field applied parallel (●) and perpendicular (○) to the chain axis. Inset: temperature dependence of ratio M/H of single crystals in the low-temperature region with the external field applied parallel (●) and perpendicular (○) to the chain axis.

It is reasonable to postulate that the magnetic anisotropy within **1a** and **1b** chains is governed by the octahedral Co^{II}. The heterometallic chains $[CoMn(PhCOO)_4]_n$ possess Ising-type anisotropy, while the material is isostructural with **1b**.[8a] The isotropic Mn^{II} spins have been substituted by fully anisotropic Co^{II}, which has induced the flip of the easy magnetization directions. Despite large similarities, the chains in **1a** and **1b** have different structures. In **1b** octahedral Co^{II} are not situated at a symmetry center and therefore the coordination sphere is much more distorted than in **1a**, which is already greatly distorted with three very differ-

ent metal–ligand bond lengths: two short (2.013 Å), two medium (2.110 Å), and two long (2.227 Å). In **1b**, there are still two short Co_O–O bond lengths (2.021 Å) which coincide with **1a**. These short distances involve the oxygen atoms of the two $\mu(\eta_1,\eta_1)$-benzoato bridges. The four other Co_O–O distances are distributed homogeneously between 2.1 and 2.25 Å (2.136, 2.169, 2.202, and 2.258 Å). These differences must be considered in parallel with the orientation of the elongated axis with respect to the chain axis, which is close to 40° in both compounds. It is clear that slight reorientation of the anisotropy axes at octahedral sites due to local distortions of the coordination sphere can produce magnetization flip from one axis to another, and may therefore explain the radical modifications of preferred magnetization orientations.

Conclusions

The method based on in-situ ligand generation has been extended to the synthesis of several 1D neutral homo- and heterometallic coordination polymers. The carboxylate-based ligands are generated from aromatic aldehydes, which are the reaction media. In these materials carboxylato bridges connect metal ions to form zigzag chain structures. Two types of chains have been characterized: a) chains with metal ions in both tetrahedral and octahedral environments; ii) chains with metal ions in tetrahedral coordination polyhedra only. In weak ligand fields, Mn^{II} is definitely located in octahedral surroundings whereas Zn^{II} or Co^{II} adapt easily to tetrahedral positions. Thus, heterometallic chains are formed of octahedra (MnO_6) and tetrahedra (ZnO_4 or CoO_4). In $[CoZn(PhCOO)_4]_n$ the structure of the chains is not a consequence of the preferred coordination polyhedra of Co^{II}. Homometallic $[Co(PhCOO)_2]_n$ and $[Co(p\text{-}MePhCOO)_2]_n$ chains are formed from both CoO_6 and CoO_4 coordination polyhedra. Zn^{II} prefers to be in a tetrahedral rather than an octahedral environment, and thus in the chain formed with Zn^{II} this ion always occupies the tetrahedral position. In choosing metal ions which like, or dislike, different coordination geometries, we can predetermine the chain structures of benzoate-based neutral 1D coordination polymers.

The magnetic properties of $[ZnMn(PhCOO)_4]_n$ are typical of Heisenberg chains with small antiferromagnetic interactions between Mn^{II} isotropic spins, which can be treated in the classical approximation. In the two forms of $[Co(PhCOO)_2]_n$ and $[Co(p\text{-}MePhCOO)_2]_n$ the superexchange interactions between metal spins are ferromagnetic, and the anisotropic nature of the spin carriers, especially octahedral Co^{II}, leads to strongly anisotropic ferromagnetic chains. The orthorhombic form shows three-dimensional magnetic ordering with $T_C = 3.7$ K due to short interchain distances, which prevent the observation of single-chain magnetic behavior. The monoclinic form does not order magnetically down to the lowest temperature; instead it shows typical single-chain magnet behavior with thermally activated relaxation process. Furthermore, it appears that tiny structural changes have dramatic consequences for the orientation of the easy axis of magnetization, which flips from the chain axis to a perpendicular direction in the two forms of $[Co(PhCOO)_2]_n$.

Experimental Section

Materials: All commercially available chemicals were used as received. Toluene and acetonitrile were purified by standard procedures before use. $[Co(PhCOO)_2]$ (**1a** and **1b**) and $[Co(p\text{-}MePhCOO)_2]$ (**2**) were synthesized according to the method described previously.[8a]

Complexes:

*$[ZnMn(PhCOO)_4]_n$ (**3**)*: $Mn(NO_3)_2{\cdot}6H_2O$ (144 mg, 0.5 mmol) was boiled in benzaldehyde (5 mL) for 5 min. Filtering of the reaction mixture from the small amount of solid was followed by addition of benzaldehyde (2 mL) and $Zn(NO_3)_2{\cdot}4H_2O$ (79 mg, 0.3 mmol) to the filtrate. The reaction mixture was heated until a white crystalline solid was deposited. Then the solution was cooled to 70–80 °C, and acetonitrile (8 mL) was added to the reaction mixture. After 1 h, the mixed-metal benzoate **3** was collected by filtration, washed with acetonitrile and ether, and dried in vacuum. Yield: 165 mg (91 %); elemental analysis calcd (%) for $MnZnC_{28}H_{20}O_8$: C 55.61, H 3.33, Mn 9.1, Zn 10.8; found: C 55.59, H 3.26, Mn 8.9, Zn 10.6.

*$[CoZn(PhCOO)_4]_n$ (**4**)*: This complex was prepared by the same procedure as for **2**,[8a] using a mixture of $Co(NO_3)_2{\cdot}6H_2O$ (582 mg, 2 mmol) and $Zn(NO_3)_2{\cdot}4H_2O$ (523 mg, 2 mmol). Blue crystals of **4** were obtained. Yield: 950 mg (82.7 %); elemental analysis calcd (%) for $CoZnC_{28}H_{20}O_8$: C 55.24, H 3.31, Co 9.7, Zn 10.7; found: C 55.39, H 3.34, Co 9.8, Zn 10.6.

Physical measurements: Elemental analyses were performed using a Carlo Erba 1106 CHN analyzer and a JEOL JSM 6400 with Oxford Instruments analysis system. Magnetizations were recorded with a Quantum Design MPMS SQUID magnetometer operating in the 2–300 K range with a DC magnetic field up to 5 T. The experimental data were corrected for the diamagnetism of the sample holder and the intrinsic diamagnetism of the materials evaluated with Pascal's tables. The single-crystal measurements were performed on an assembly of five to ten needle-shaped single crystals. Single crystals were checked individually and aligned by X-ray diffraction. For both **1a** and **1b** the elongated axis of the needles coincided with the chain axes *c* and *a*, respectively. Magnetization measurements for powders of **3** are given in the Supporting Information with the best-fit curve. Sub-kelvin AC susceptibility measurements were performed on a modified Oxford Instruments 3He Heliox cryostat equipped with a 5 T magnet, and a homemade AC probe by courtesy of Prof. M. Novak (UFRJ, Rio de Janeiro, Brazil): available temperature range 280–2000 mK, frequency range 20–15 000 Hz, for oscillating field excitations up to 0.33 Oe. For **1a**, measurements were performed in the 330–1650 mK range using 12 logarithmically spaced frequencies from 30 to 9000 Hz with an excitation field of 0.235 Oe.

Crystallographic data collection and structure determination: Single crystals were mounted on a Nonius four-circle diffractometer equipped with a CCD camera and a graphite monochromatic $Mo_{K\alpha}$ radiation source ($\lambda = 0.71073$ Å), from the Centre de Diffractométrie (CDFIX), Université de Rennes 1, France. Data were collected at 293 K. Structures were solved by direct methods using the SHELXS-97 program and refined by the full-matrix least-squares method on F^2 using the SHELXL-97 program.[22] For **3**, the refinements of the occupancy factors of the metal sites led to a random distribution of Zn and Co ions on the two sites. The occupation factor of each cation was then fixed to 0.5, and the same anisotropic displacement parameters were used for the two cations sharing the same site. Crystallographic data are summarized in Table 2. CCDC 627240, CCDC 627241, and CCDC 627242 contain the supplementary crystallographic data for this paper. These data can be obtained free of charge from Cambridge Crystallographic Data Centre via www.ccdc.cam.ac.uk/data_request/cif.

Acknowledgements

Financial support from the CNRS, the Région Bretagne, INTAS grant 03-51-4532, and the EC through the Consortium INSTM-NE-MAGMA-NET (FP6-NMP3-CT-2005-515767). K.B acknowledges support from the EC and the Human Potential Program RTN-QUELMOLNA (MRTN-CT-2003-504880). This work was partially supported by the joint CNRS–National Academy of Sciences of Ukraine Grants Program.

[1] a) P. Przychodzén, T. Korzeniak, R. Podgajny, B. Sieklucka, *Coord. Chem. Rev.* **2006**, *250*, 2234–2260; b) M. Dan, C. N. R. Rao, *Angew. Chem.* **2006**, *118*, 287–291; *Angew. Chem. Int. Ed.* **2006**, *45*, 281–285; c) A. Beghidja, P. Rabu, G. Rogez, R. Welter, *Chem. Eur. J.* **2006**, *12*, 7627–7638; d) H. Miyasaka, R. Clérac, *Bull. Chem. Soc. Jpn.* **2005**, *78*, 1725–1748; e) P. D. C. Dietzel, Y. Morita, R. Blom, H. Fjellvåg, *Angew. Chem.* **2005**, *117*, 6512–6516; *Angew. Chem. Int. Ed.* **2005**, *44*, 6354–6358; f) C. N. R. Rao, S. Natarajan, R. Vaidhyanathan, *Angew. Chem.* **2004**, *116*, 1490–1521; *Angew. Chem. Int. Ed.* **2004**, *43*, 1466–1496; ; g) S. Kitagawa, R. Kitaura, S.-I. Noro, *Angew. Chem.* **2004**, *116*, 2388–2430; *Angew. Chem. Int. Ed.* **2004**, *43*, 2334–2375.

[2] a) S. Viswanathan, A. de Bettencourt-Dias, *Inorg. Chem. Commun.* **2006**, *9*, 444–448; b) L. Wen, Y. Li, D. Dang, Z. Tian, Z. Ni, Q. Meng, *J. Solid State Chem.* **2005**, *178*, 3336–3341; c) R. Fu, S. Xiang, S. Hu, L. Wang, Y. Li, X. Huang, X. Wu, *Chem. Commun.* **2005**, *42*, 5292–5294.

[3] a) A. Cingolani, S. Galli, N. Masciocchi, L. Pandolfo, C. Pettinari, A. Sironi, *J. Am. Chem. Soc.* **2005**, *127*, 6144–6145; b) S. Takamizawa, T. Saito, T. Akatsuka, E.-I. Nakata, *Inorg. Chem.* **2005**, *44*, 1421–1424.

[4] O. Hallale, S. A. Bourne, K. R. Koch, *New J. Chem.* **2005**, *29*, 1416–1423.

[5] a) Y.-Z. Zheng, M.-L. Tong, W.-X. Zhang, X.-M. Chen, *Angew. Chem.* **2006**, *118*, 6458–6462; *Angew. Chem. Int. Ed.* **2006**, *45*, 6310–6314; b) X.-T. Liu, X.-Y. Wang, W.-X. Zhang, P. Cui, S. Gao, *Adv. Mater.* **2006**, *18*, 2852–2856; c) R. Lescouëzec, L. M. Toma, J. Vaissermann, M. Verdaguer, F. S. Delgado, C. Ruiz-Pérez, F. Lloret, M. Julve, *Coord. Chem. Rev.* **2005**, *249*, 2691–2729; d) T. Kajiwara, M. Nakano, Y. Kaneko, S. Takaishi, T. Ito, M. Yamashita, A. Igashira-Kamiyama, H. Nojiri, Y. Ono, N. Kojima, *J. Am. Chem. Soc.* **2005**, *127*, 10150–10151; e) M. Ferbinteanu, H. Miyasaka, W. Wernsdorfer, K. Nakata, K.-I. Sugiura, M. Yamashita, C. Coulon, R. Clérac, *J. Am. Chem. Soc.* **2005**, *127*, 3090–3099; f) J. Yoo, W. Wernsdorfer, E.-C. Yang, M. Nakano, A. L. Rheingold, D. N. Hendrickson, *Inorg. Chem.* **2005**, *44*, 3377–3379; g) J.-P. Costes, J. M. Clemente-Juan, F. Dahan, J. Milon, *Inorg. Chem.* **2004**, *43*, 8200–8202; h) A. Caneschi, D. Gatteschi, N. Lalioti, C. Sangregorio, R. Sessoli, G. Venturi, A. Vindigni, A. Rettori, M. G. Pini, M. A. Novak, *Angew. Chem.* **2001**, *113*, 1810–1813; *Angew. Chem. Int. Ed.* **2001**, *40*, 1760–1763; i) Z.-M. Sun, A.-V. Prosvirin, H.-H. Zhao, J.-G. Mao, K.-R. Dunbar, *J. Appl. Phys.* **2005**, *97*, 10B305/1–10B305/3; j) A.-V. Palii, S. M. Ostrovsky, S. I. Klokishner, O. S. Reu, Z.-M. Sun, A.-V. Prosvirin, H.-H. Zhao, J.-G. Mao, K.-R. Dunbar, *J. Phys. Chem. A* **2006**, *110*, 14003–14012.

[6] a) T. K. Maji, W. Kaneko, M. Ohba, S. Kitagawa, *Chem. Commun.* **2005**, 4613–4615; b) R. D. Poulsen, A. Bentien, M. Chevalier, B. B. Iversen, *J. Am. Chem. Soc.* **2005**, *127*, 9156–9166; c) S. C. Manna, E. Zangrando, A. Bencini, C. Benelli, N. R. Chaudhuri, *Inorg. Chem.* **2006**, *45*, 9114–9122; d) J. Jia, X. Lin, A. J. Blake, N. R. Champness, P. Hubberstey, L. Shao, G. Walker, C. Wilson, M. Schröder, *Inorg. Chem.* **2006**, *45*, 8838–8840; e) Y. J. Kim, Y. J. Park, D.-Y. Jung, *Dalton Trans.* **2005**, 2603–2608; f) S. H. Jhung, J.-H. Lee, P. M. Forster, G. Férey, A. K. Cheetham, J.-S. Chang, *Chem. Eur. J.* **2006**, *12*, 7899–7905.

[7] a) M. Spohn, J. Strähle, *Z. Naturforsch. B* **1988**, *43*, 540–546; b) H. Kumagai, M. Ohba, K. Inoue, H. Ōkawa, *Chem. Lett.* **2002**, 1006–1007; c) G. A. Guseynov, F. N. Musaev, B. T. Usubaliev, I. R. Amirsalanov, Kh. S. Mamedov, *Koord. Khim.* **1984**, *10*, 117–122.

[8] a) K. S. Gavrilenko, S. V. Punin, O. Cador, S. Golhen, L. Ouahab, V. V. Pavlishchuk, *J. Am. Chem. Soc.* **2005**, *127*, 12246–12253; b) K. S. Gavrilenko, S. V. Punin, O. Cador, S. Golhen, L. Ouahab, V. V. Pavlishchuk, *Inorg. Chem.* **2005**, *44*, 5903–5910.

[9] C. Ruiz-Pérez, J. Sanchiz, M. Hernández-Molina, F. Lloret, M. Julve, *Inorg. Chim. Acta* **2000**, *298*, 202–208.

[10] a) V. Tangoulis, D. A. Malamatari, K. Soulti, V. Stergiou, C. P. Raptopoulou, A. Terzis, T. A. Kabanos, D. P. Kessissoglou, *Inorg. Chem.* **1996**, *35*, 4974–4983; b) B. Albela, M. Corbella, J. Ribas, I. Castro, J. Sletten, H. Stoeckli-Evans, *Inorg. Chem.* **1998**, *37*, 788–798; c) G. Fernandes, M. Corbella, J. Mahia, M. A. Maestro, *Eur. J. Inorg. Chem.* **2002**, 2502–2510; d) S. G. Baca, Y. Sevryugina, R. Clérac, I. Malaestean, N. Gerbeleu, M. A. Petrukhina, *Inorg. Chem. Commun.* **2005**, *8*, 474–478; e) C. J. Milios, T. C. Stamatatos, P. Kyritsis, A. Terzis, C. P. Raptopoulou, R. Vicente, A. Escuer, S. P. Perlepes, *Eur. J. Inorg. Chem.* **2004**, 2885–2901.

[11] M. E. Fisher, *Am. J. Phys.* **1964**, *32*, 343–346.

[12] A. Abragam, B. Bleaney, *Electron Paramagnetic Resonance of Transition Ions*, Dover, New York, **1970**.

[13] a) J. M. Clemente-Juan, E. Coronado, A. Forment-Aliaga, J. R. Galán-Mascarós, C. Giménez-Saiz, C. J. Gómez-García, *Inorg. Chem.* **2004**, *43*, 2689–2694; b) H. Andres, J. M. Clemente-Juan, R. Basler, M. Aebersold, H.-U. Güdel, J. J. Borrás-Almenar, A. Gaita, E. Coronado, H. Büttner, S. Janssen, *Inorg. Chem.* **2001**, *40*, 1943–1950.

[14] a) D. Gatteschi, R. Sessoli, *Angew. Chem.* **2003**, *115*, 278–309; *Angew. Chem. Int. Ed.* **2003**, *42*, 268–297; b) D. Gatteschi, R. Sessoli, J. Villain, *Molecular Nanomagnets*, Oxford University Press, Oxford, **2006**; c) C. Coulon, H. Miyasaka, R. Clérac, *Struct. Bonding* **2006**, *122*, 163–206.

[15] C. Coulon, R. Clerac, L. Lecren, W. Wernsdorfer, H. Miyasaka, *Phys. Rev. B* **2004**, *69*, 132408/1–132408/4.

[16] O. Kahn, *Molecular Magnetism*, VCH, Weinheim, **1993**.

[17] J. Curely, R. Georges, M. Drillon, *Phys. Rev. B* **1986**, *33*, 6243–6252.

[18] R. J. Glauber, *J. Math. Phys.* **1963**, *4*, 294–307.

[19] a) R. Lescouëzec, J. Vaissermann, C. Ruiz-Perez, F. Lloret, R. Carrasco, M. Julve, M. Verdaguer, Y. Dromzee, D. Gatteschi, W. Wernsdorfer, *Angew. Chem.* **2003**, *115*, 1521–1524; *Angew. Chem. Int. Ed.* **2003**, *42*, 1483–1486; b) T. Liu, D. Fu, S. Gao, Y. Zhang, H. L. Sun, G. Su, Y. Liu, *J. Am. Chem. Soc.* **2003**, *125*, 13976–13977; c) L. M. Toma, R. Lescouezec, F. Lloret, M. Julve, J. Vaissermann, M. Verdaguer, *Chem. Commun.* **2003**, 1850–1851; d) E. Pardo, R. Ruiz-Garcia, F. Lloret, J. Faus, M. Julve, Y. Journaux, F. Delgado, C. Ruiz-Perez, *Adv. Mater.* **2004**, *16*, 1597–1600; e) A. Maignan, V. Hardy, S. Hebert, M. Drillon, M. R. Lees, O. Petrenko, D. M. Paul, D. Khomskii, *J. Mater. Chem.* **2004**, *14*, 1231–1234; f) M. Ferbinteanu, H. Miyasaka, W. Wernsdorfer, K. Nakata, K. Sugiura, M. Yamashita, C. Coulon, R. Clerac, *J. Am. Chem. Soc.* **2005**, *127*, 3090–3099; g) L. M. Toma, R. Lescouëzec, J. Pasàn, C. Ruiz-Pérez, J. Vaissermann, J. Cano, R. Carrasco, W. Wersndorfer, F. Lloret, M. Julve, *J. Am. Chem. Soc.* **2006**, *128*, 4842–4853; h) L. Bogani, C. Sangregorio, R. Sessoli, D. Gatteschi, *Angew. Chem.* **2005**, *117*, 5967–5971; *Angew. Chem. Int. Ed.* **2005**, *44*, 5817–5821; i) K. Bernot, L. Bogani, A. Caneschi, D. Gatteschi, R. Sessoli, *J. Am. Chem. Soc.* **2006**, *128*, 7947–7956; j) K. Bernot, L. Bogani, D. Gatteschi, R. Sessoli, *Inorg. Chim. Acta* **2007**, *360*, 3807–3812.

[20] K. S. Cole, R. H. Cole, *J. Chem. Phys.* **1941**, *9*, 341–347.

[21] J. A. Mydosh, *Spin Glasses: An Experimental Introduction*, Taylor & Francis, London, **1993**.

[22] G. M. Sheldrick, SHELX-97, University of Göttingen, Göttingen (Germany), **1997**.

Received: August 24, 2007
Published online: December 28, 2007

